Motor Compositionality and Timing: Combined Geometrical and Optimization Approaches

Tamar Flash, Matan Karklinsky, Ronit Fuchs, Alain Berthoz, Daniel Bennequin and Yaron Meirovitch

Abstract Human movements are characterized by their invariant spatiotemporal features. The kinematic features and internal movement timing were accounted for by the mixture of geometries model using a combination of Euclidean, affine and equi-affine geometries. Each geometry defines a unique parametrization along a given curve and the net tangential velocity arises from a weighted summation of the logarithms of the geometric velocities. The model was also extended to deal with geometrical singularities forcing unique constraints on the allowed geometric mixture. Human movements were shown to optimize different costs. Specifically, hand trajectories were found to maximize motion smoothness by minimizing jerk. The minimum jerk model successfully accounted for a range of human end-effector motions including unconstrained and path-constrained trajectories. The two modeling approaches involving motion optimality and the geometries' mixture model are here further combined to form a joint model whereby specific compositions of geometries can be selected to generate an optimal behavior. The optimization serves to define the timing along a path. Additionally, new notions regarding the nature

T. Flash · M. Karklinsky · R. Fuchs
Department of CS and Applied Mathematics, Weizmann Institute of Science, Rehovot, Israel
e-mail: tamar.flash@weizmann.ac.il

M. Karklinsky
e-mail: matan.karklinsky@weizmann.ac.il

R. Fuchs
e-mail: ronit.fuchs@gmail.com

A. Berthoz
College de France, Paris, France
e-mail: alain.berthoz@gmail.com

D. Bennequin
Institut de Mathématiques de Jussieu, Paris 7, Paris, France
e-mail: bennequin@math.univ-paris-diderot.fr

Y. Meirovitch (✉)
Department of Computer Science and Artificial Intelligence Laboratory, MIT,
77 Massachusetts Ave, 02139 Cambridge, MA, USA
e-mail: yaron.mr@gmail.com

G. Venture et al. (eds.), *Biomechanics of Anthropomorphic Systems*, Springer Tracts in Advanced Robotics 124, https://doi.org/10.1007/978-3-319-93870-7_8

of movement primitives used for the construction of complex movements naturally arise from the consideration of the two modelling approaches. In particular, we suggest that motion primitives may consist of affine orbits; trajectories arising from the group of full-affine transformations. Affine orbits define the movement's shape. Particular mixtures of geometries achieve the smoothest possible motions, defining timing along each orbit. Finally, affine orbits can be extracted from measured human paths, enabling movement segmentation and an affine-invariant representation of hand trajectories.

1 Introduction

1.1 Organizing Principles of Human Task Space Kinematics

Many of the fundamental ideas underlying our current understanding of human movement generation arise already when examining how humans control their hand trajectories, the hand being the end-effector of the upper limb. Despite the high dimensionality and complex mechanics inherent in any human action, the movements of a multi-degrees of freedom limb such as the upper arm, can be investigated by focusing on the motions of a single disembodied point moving through space and time [7]. This approach may seem simplistic at first. However, as has already been demonstrated by many earlier studies, fundamental questions addressing different perspectives of the problem of movement generation can be addressed and even resolved at the level of the end-effector motion.

The first issue addressed here is that of overcoming or resolving the redundancy existing at the task level; any end-effector movement can be performed in many different ways. How does the motor system select distinct trajectories when the space of all possible alternative movements is so high dimensional? Interestingly, even in the case of two dimensional hand trajectories, redundancy issues arise. Moving the tip of a pen from one point to another can be performed via an infinite-dimensional set of possible paths. The temporal aspect of movement generation introduces an additional dimension that the motor system has to deal with. Not only does the movement duration have to be selected, but also does the instantaneous movement speed. The selection or planning of a particular hand speed profile creates a specific relation between path geometry and time. Thus, a closer inspection of the task of controlling two-dimensional (2D) end-effector movements reveals the richness of possible choices. Such choices are reflected in both the geometrical features and the timing pattern chosen by the motor system when performing motor actions. When inspecting higher dimensional movements from the perspectives of joint kinematics and dynamics, the basic question of selecting a specific action out of the vast set of possible ones essentially remains the same, but is even more complicated.

To select one possible movement among the very large set of possible ones, the notion of optimality serves as a key concept. We do tend to think of human movement as being optimal, but in what sense? When examining end-effector kinematics, evidence has accumulated indicating that human movements are first and foremost kinematically optimal; that the hand trajectory, referring to both the hand path and its velocity profile, maximizes smoothness. This objective was expressed by the minimization of some integrated squared n-th order time derivative of hand position [23, 38, 51, 56]. The lowest order time derivative of position is velocity, then acceleration, then jerk, snap, etc. Even for two-dimensional hand trajectories in the horizontal plane, seemingly simple optimization cost functions yield a surprisingly rich set of possible behaviors. Free reaching movements are predicted to follow straight hand paths with single-peaked bell speed profiles [1, 42]. Obstacle avoidance or simple curved movements were successfully modeled by introducing via-points, i.e., additional points through which the hand should pass [23]. Other similar approaches were applied to model more complex behaviors, including drawing movements or path tracking movements. Thus, applying additional task constraints can redefine the optimal behavior and form more and more complex behaviors. Positions that must be passed through [23], prescribed paths [51, 56], timing requirements [54] and online trajectory corrections [21, 33, 38], may all be incorporated into the minimization of some kinematic cost. Thus, the relatively simple notion that a movement is optimal in some sense can be used to generate a diverse set of movements.

Inspecting the notion of optimization as a possible motion planning principle, however, reveals some problems. Deriving an optimal solution cannot always be carried out, especially online motion planning purposes or when time is pressing, such as in the case of required online corrections [38, 57]. When the complexity of the movement task increases, several additional difficulties arise. Computationally, it becomes harder to find an optimal action. Moreover, storing in memory all possible optimal paths and trajectories does not provide a satisfactory solution since it requires a massive memory storage capacity.

Given these difficulties, another possible solution to the motion control problem arises from another underlying notion, that of compositionality [10, 11, 2, 22, 43]. According to this notion, most movements result from the composition of elementary building blocks, i.e. motion primitives. The problem, however, is how it is possible to identify such discrete primitives from apparently continuous movements? Additionally, what exactly is meant by the term motion primitive? For instance, can a large space of different behaviors be spanned based only on the use of a smaller number of motion templates?

Consider, for example, the simplest candidates, straight strokes. These strokes are the first that come to mind given the relatively straight paths and the bell-shaped velocity profiles characterizing reaching movements [1, 42]. These straight geometric paths are traversed with stereotypical bell shaped velocity profiles. However, even in the case of simple straight hand motion primitives, the number of such possible strokes is huge. The stroke's orientation, amplitude, and duration are three free parameters. Hence, the space of possible stroke primitives is large. Is each stroke represented by a separate motor plan? The similarity of the normalized speed profiles of different strokes suggests that this option is less likely than the possibility that a motion primitive exists; namely, given a generic motor template and the specific orientation, amplitude, and duration of the required movement, these are sufficient for forming specific required strokes. Furthermore, it appears that movement durations and amplitudes are correlated. Such coupling happens when it is required to move as rapidly and as accurately as possible, i.e., when movement duration depends on its amplitude and on the target's width (Fitts's law; [18]). Hence, in general, the task of reaching between given end-points requires the specification of either three or only two parameters out of the three possible ones.

The above observations concerning straight movement primitives should also be considered from a different perspective. Straight strokes are inherently invariant; irrespectively of their amplitude, duration and orientation. The normalized speed profile of a straight stroke is bell-shaped and is roughly the same across different movement end-point locations and durations, at least in the case of 2D movements in the horizontal plane. In three-dimensional space the paths are less straight and do depend on the end-point locations, which has led to the suggestion that different motion planning strategies subserve 3D versus 2D movements [8, 9, 14].

Hence, given the above arguments, we find that invariance is another fundamental concept in trajectory formation, which goes hand in hand with the ability of the system to generalize a motor plan designed for a specific task in order to accomplish similar tasks. What types of invariants characterize the spatiotemporal features of end-effector motions? The low dimensionality of task space offers a suitable ground for carrying a geometric analysis of movements based on geometrical symmetries and invariance theory. Note that geometrical principles for the planning and execution of complex movements of different body segments were recently presented in a paper by Bennequin and Berthoz [6].

The study of the action of a transformation group operating either in the plane or in 3D space can provide insights into the geometrical principles guiding human motor control. Affine transformations are the point-by-point correspondences sending straight lines to straight-lines; the equi-affine transformations, in addition, are respecting a unit of area in 2D (resp. volume in 3D). Humans move the hand through 2D task space with kinematics that indicate equi-affine invariance, following a motion regularity called the two-thirds power law [34]. This law states that the movement speed is proportional to the end-effector path curvature, raised to the power $-1/3$, thus specifically slowing down along the curvier sections of the path [27, 46]. Isochrony, the tendency of movement speed to be modified such that movement durations are relatively unaffected by the movement's Euclidean extent is another invariance that can furtherly be interpreted within the realm of full-affine invariance of motor behavior [5].

In this chapter, we discuss a few different approaches to modeling human trajectory formation. One approach involves optimization models. Another approach involves using geometrically based descriptions. We show how these two approaches can be combined to address both the spatial and temporal aspects of end-effector trajectory planning. Regarding optimization models, we focus on the minimum jerk model. We thoroughly discuss geometry–based models using non-Euclidean (in the sense of groups, not in the sense of metrics) geometries. We first briefly review the relation between equi-affine geometry based models and the two-thirds power law.

We then proceed to review the mixture of geometries model. This model is a unifying model that suggests that movement is generated not only based on a single geometry but on a multiplicative mixture (see below) of three geometries, namely Euclidean geometry and the two non-Euclidean ones: affine and equi-affine geometries. Thus, it was suggested that movement speed (tangential velocity) emerges from a mixture of speeds, each being constant within its associated geometry. These geometric speeds are combined, dictating the net speed and timing of the movement. The model also assumes different possible combinations of the three geometrical speeds, characterized by the different weighted contributions of the three geometries to the actual movement. The relation between the mixture weight parameters and task optimality has not yet been sufficiently investigated but here we advance the possibility that both optimization and geometric mixtures may explain the observed kinematic behavior. One possibility is that the mixture of different geometries is formed to generate the smoothest possible movement. To examine whether this indeed can be the case, movements along several exemplary paths were examined, and their velocity profiles were modeled.

We compare the properties of the mixed geometry model to simpler models; in particular, a mixed geometric parameter allows moving through inflection points without having a singularity [5]. Its free parameters (the weights of the three geometries) are constrained to follow certain mathematically simple relationships at the singularity points for the velocities not to become infinitely large. We use the mixed geometry model to account for experimental data of both hand drawing and locomotion trajectories. The free weight parameters were selected among all possible weight parameters in order to achieve the best fit of the predicted velocity profiles to the experimental data as well as sufficient constancy of the weight parameters during long enough temporal intervals [5]. Based on these calculations, several observations on the possible mixtures of geometries used to generate different trajectories are discussed. Inspecting the free parameters (weights) that account for the experimental data, we found that different alternative mixtures might result in quite similar velocity profiles, which were practically indistinguishable across different mixtures.

Continuing our interest in geometric invariance, we also examine a set of plausible candidate geometric motion primitives and describe how these primitives may emerge based on the main notions of invariance and optimization. In particular, following Meirovitch [39] we propose that these primitives could geometrically correspond to the affine orbits; geometric orbits resulting from the combined actions of the Euclidean, equi-affine and full-affine transformation groups on points in the plane. The speed profile along primitive affine orbits may satisfy both the mixed geometry and the minimum jerk models, yielding motions that are both invariant and maximally smooth. We also discuss how affine orbits can be used for the segmentation of experimentally recorded end-effector trajectories.

2 Modeling Task Space Kinematics Using Optimization Principles

2.1 *The Minimum Jerk Model Defining the Smoothest Trajectory*

The optimality of movement based on the minimum jerk model states that a trajectory $r(t) = (x(t), y(t))$ is optimal in the sense that the cumulative squared jerk, i.e., the squared jerk cost integrated over the entire movement duration, is minimal:

$$J = \int_0^T \left(\dddot{x}^2 + \dddot{y}^2\right) dt$$

The minimum jerk model enables to predict how the motor system operates under different task requirements such as the generation of point-to-point reaching or obstacle-avoidance movements [19, 23].

For point-to-point movements, given some boundary conditions, the two-dimensional trajectory predicted by this jerk minimization model is such that $x(t)$ and $y(t)$ are fifth order time polynomials. In the simplest case of zero speed and acceleration at the movement start-point and end-point, the resulting trajectories are straight paths with symmetric bell-shaped velocity profiles, closely resembling stereotypical human behavior.

To model curved trajectories, the movements were assumed to start at some initial point, pass through one or several additional intermediate points (termed via-points), and end at some specified end-point. For example, using the minimum jerk model, the optimization process predicts the movement that should be generated between the initial and final positions while passing through each via-point along the way at an a priori unspecified time. The solution of this minimization problem defines the movement between each pair of consecutive points as a 5th order time-dependent polynomial, with equality position constraints obeyed by the movement segments on both sides of each via-point. The model predicts the path geometry and full kinematic profile including internal timing.

For various applications, it is sometimes more helpful to examine the jerk cost after some normalization. For instance, if we assume a movement duration T and an amplitude S to be specified, then a normalized version, the unit-less normalized jerk, can be defined $J_N = \frac{T^6}{S^2} J$ as which makes it easier to compare and examine the jerk costs across different movement shapes. Other approaches to normalize the jerk cost were based, for example, on the spectral arc-length metric [3].

For a given path, path-constrained optimization deals with the problem of finding the optimal speed profile along the prescribed path [51, 56]. The predicted speed profile, the solution of the path-constrained optimization problem, is specifying the dependency of the end-effector speed on the path shape (geometry).

The relations between the predictions arising from optimization and those resulting from equi-affine invariance, which we discuss next, were examined from different perspectives [24, 27, 39, 49, 51, 60]. It is interesting to mention that the equi-affine parametrization (i.e. the two-thirds power law) corresponds to the case where the jerk vector $\left(\dddot{x}(t), \dddot{y}(t)\right)$ is proportional to the velocity vector $(\dot{x}(t), \dot{y}(t))$. Possible extensions of the minimum jerk model naturally arise if one examines the time derivatives of some order k being different from $k = 3$ which relates to the time derivative of position, i.e., jerk used in the minimum jerk model. The minimum acceleration model, with $k = 2$ was also used to model human behavior during reaching tasks [4]. The minimum acceleration cost also appears to be a good candidate for describing human locomotion [41]. The minimum snap model with $k = 4$ was used as an underlying optimization cost for the control algorithm of robotic quadcopter swarms [40] as well as for object manipulation movements [16].

A more general extension comes when the cost arising from Euclidean jerk or acceleration is replaced with a cost arising from Riemannian metrics used on the configuration manifold describing the configuration of the human arm. This approach was developed by Biess et al. [9]. In their study, the geodesics of the integrated kinetic energy cost were used to predict the optimal geometric movement paths, and the velocities along these geodesics were dictated based on the minimization of the third derivative of the Euclidean distance with respect to time when moving along the resulting optimal paths.

2.2 *Invariance Achieved Through Power Laws and Isochrony*

As described above, point-to-point reaching movements are both spatially and temporally invariant. Invariance in movement generation applies to more than just reaching movements. Other examples are curved and scribbling movements. In particular, we consider the two-thirds power law describing how the geometry and timing of curved human movements are related. The influence of path geometry on timing is modeled by the two-thirds power law: $\omega = C\kappa^{2/3}$, relating angular speed ω to curvature κ [34]. An equivalent formulation of the two-thirds power law is:

$$v = \gamma\kappa^{-\beta}$$

relating tangential velocity (speed) v with curvature κ, with exponent whose value is: $\beta = \frac{1}{3}$, and with γ being the piecewise constant named the velocity gain factor. This law captures the phenomenon that human movement speeds slow down during more curved segments of the trajectories.

The two-thirds power law or similar power laws were found in smooth pursuit eye movements [15], full body locomotion [29, 61], leg motions [31], speech [55] visual perception of motion [36, 59] and motor imagery [32].

Other studies have shown that a generalized form of a power law holds for shapes other than ellipses and those originally tested, and that the value of the power law exponent depends on the shape of the movement path. Maximization of smoothness through the minimum jerk model or other minimum squared derivatives models successfully predicted the power law values [51]. These predictions included the power law exponent values, based on the order of the time derivative of position used by the minimum squared derivatives model and the value of the curvature modulation frequency [30].

Another approach initially used to account for the two-thirds power law was based on a geometrical approach, specifically showing that the two-thirds power law is equivalent to the movement having a constant equi-affine speed [27, 46]. Equi-affine speed designated the time derivative of equi-affine arc-length which is mathematically defined as $d\sigma/dt$, the derivative of equi-affine arc-length distance with respect to time, where the equi-affine arc-length distance is defined as: $\sigma = \int \kappa^{1/3} ds$, s being the Euclidean arc-length distance [20, 25, 27]. Differentiating both sides of the last mathematical expression with respect to time and assuming that the equi-affine speed is constant, corresponding to the velocity gain factor $\frac{d\sigma}{dt} = \gamma$, results in the two-thirds power law [20].

The importance of the equi-affine description lies not only in enabling to express the two-thirds power law in geometrical terms but also in suggesting a geometrical framework for the description of human motion. The formulation of the relation between the two-thirds power law and constant equi-affine speed enabled to formulate the idea that a possible mathematical framework for analyzing movement similarities and invariance might involve the introduction of group theory and the moving frame method [5, 20]. The use of group theory enables to consider the movement along a given trajectory by repeatedly applying some incremental transformation on the end-effector position. Similarly, using one member of a group of transformations it is possible to transform one motion into another and to compare among different differential invariants. Mainly, the generalizations of arc-lengths and curvatures according to each geometry should remain the same (invariant), when operated on by a member of this specific group of transformations (seen as a symmetry of the geometry, which is defined by the group).

Another important variable that characterizes movements is their total duration, and a significant question in studying motor control is how the brain selects the durations for different movements. In this context, it is pertinent to describe a second important behavioral characteristic of human motion, namely global isochrony. The total durations of human movements sub-linearly depend on movement amplitudes; when two figural forms, differing only in their spatial scales, are drawn, they have roughly equal durations [60, 62]. Related temporal regularities also appear in the production of goal directed movements, such as movements constrained to pass through via-points. In this case, the durations between the movement's start and via-point and between the via-point and end-point are nearly equal, a phenomenon that was termed local isochrony [60, 62] and was successfully captured by the minimum jerk model [23].

3 Mixed Geometry as a Unifying Model of Task Space Invariance

While the equi-affine description has accounted for the two-thirds power law, it does not account for global isochrony. Moreover, no theory currently exists explaining how movement duration is selected, even if it does follow the two-thirds power law. Hence, to deal with these issues and to suggest a more comprehensive theory, the findings presented here regarding invariance of motor actions were integrated into a unifying model, the mixed geometry model [5]. This theory of movement generation is based on movement invariance with respect to three families of geometric transformations; the three classical transformation groups of full-affine, equi-affine, and Euclidean transformations.

Full-affine transformations include translations, rotations, dilatations, stretching and shearing. They do not preserve angles or distances but preserve only parallelisms of lines and their incidence. Equi-affine transformations are a subgroup of affine transformations that preserve area, and Euclidean transformations (also called rigid transformations) include translations and rotations and preserve lengths and angles. The importance of the three mixed geometries arises from their relations to the observed features of human motion. The full-affine speed is of importance because it provides a theoretical prediction of the isochrony principle; full-affine transformations preserve the affine arc-length of curved segments, and if full-affine speed is constant then it preserves the movement time across different affine transformations. Hence it predicts global isochrony, namely the maintenance of global duration [5]. The equi-affine geometry provides a theoretical formulation of the two-thirds power law by stating that the equi-affine speed of a movement is constant, which is equivalent to moving according to the two-thirds power law. The constancy of Euclidean speed is natural because the Euclidean metrics of space have a physical meaning since they correspond to the accepted notion of distance. The motor system is not fully invariant to non-Euclidean full-affine and equi-affine transformations, and it is not categorically invariant to Euclidean transformations since in many tasks motion time sub-linearly scales with extent. Hence, these three geometries must be combined through the mixture model, which allows accounting for the observed phenomena across a broad variety of movements and tasks.

The mixed geometry model states that movement properties are best represented by a mixture of the three geometries, full-affine, equi-affine, and Euclidean. Given the strong dependency of movement time and local kinematics on geometry, it is assumed that within each geometry the geometrical speed is constant. Hence, movement duration is proportional to the canonical invariant parameter within that particular geometry. We then assume that the time differential arises from the mixture of the three time differentials, each associated with its own geometry, with some fixed weights, represented by a trio of weight parameters.

A graphical way to imagine this would be of three different length differentials which are combined by the motor system using some constant weights to form a combined new length differential. With a slight abuse of notation, we denote this new mixture length by z which represents a mixture of arc lengths arising naturally from the three transformation groups. For ρ the full-affine arc length, σ the equi-affine arc-length and s the Euclidean (standard) arc length, z is some mixture of their values:

$$dz = d\rho^{\beta_0} d\sigma^{\beta_1} ds^{\beta_2}$$

The combination of the $\beta' s$ coefficients form a convex sum; their sum is 1 (to be compatible with the division by the time differential dt) and they are all non-negative. We will denote the trio β_0, β_1, β_2, corresponding to the full-affine, equi-affine and Euclidean weight parameters by $\bar{\beta}$, termed the mixture trio weights parameter. The mixed geometry model goes beyond the geometric description and states that the movement speed corresponding to the time derivative of the mixed geometry length parameter is proportional to dt is constant. Given that each of the arc-lengths depends on its own curvature we obtain:

$$\begin{aligned} v_0 &= C_0 \kappa^{-\frac{1}{3}} |k_1| \\ v_1 &= C_1 \kappa^{-\frac{1}{3}} \qquad \text{; where the total sum of the three exponents is equal to 1.} \\ v_2 &= C_2 \end{aligned}$$

where v_0 is the Euclidean velocity under constant full-affine speed, v_1 is the Euclidean velocity under constant equi-affine speed and v_2 is constant Euclidean velocity. The Euclidean and equi-affine curvatures are marked by κ and k_1, respectively, and the different C_i-s are the constant geometrical speeds, each associated with its own geometry while the β_i-s are the corresponding weights. Using the expressions above which define each of the speeds as a function of the specific geometric curvature, the mathematical expression for the motion speed according to the mixed geometry is then:

$$v = v_0^{\beta_0} v_1^{\beta_1} v_2^{\beta_2}$$

where the three non-negative exponents sum to one.

3.1 The Geometric Singularities

The two-thirds power law has one main drawback as a generative model for motion speed along arbitrary paths. Inflections points, having zero Euclidean curvature $\kappa = 0$, are not traceable using the two-thirds power law; the zero curvature yields infinite speed when passing through an inflection point. Thus, the model is limited to the generation of movements that only wind in one direction, namely, movements that may not turn back and wind to the opposite direction (e.g., from the anti-clockwise to the clockwise directions). Augmenting the mixed geometry model with singularity analysis leads to specific mixture weights, $\bar{\beta}$, which are required to guarantee finite nonzero speeds through singularities [5]. To traverse inflection points with $\kappa = 0$, the trio $\bar{\beta}$, must satisfy the relation:

$$\beta_1 = 3\beta_0.$$

Parabolic points, defined as points of zero equi-affine curvature can be traversed with any mixing parameter that has no full-affine component:

$$\beta_0 = 0.$$

This ability of the mixed geometry model to enable travelling through singularity points suggests a new interpretation of the role these points play in forming human movement. Rather than being break points of the motor plan, as suggested, for instance, by Viviani and Cenzato [58], the singularity points are best considered as some sort of via-points; points that the system must travel through with specific constraints on its parameters [5, 39], but without stopping nor re-planning. This type of via-points, however, assumes a different constraint than the one assumed at via-points by the minimum jerk model. Such constraints go hand in hand with the idea that continuity is guaranteed when moving through some intermediate points and that the segmented appearance of movements may not necessarily imply segmented control [52]. To summarise, the geometric singularities discussed here play a different role compared to cusps and movement end-points, when it comes to human motor control.

3.2 Motion Primitives Predicted by the Mixture of Geometries Model

The two candidate geometric movement primitives discussed so far were straight and parabolic segments [20, 27, 49]. Movement primitives, however, may have additional predefined geometric shapes, which might be accompanied by a kinematic rule prescribing the speed of movement along these geometric paths.

Straight movements are known to be the default mode of executing point-to-point movements. The nearly straight paths are traveled with a bell shaped speed profile, which could result from jerk minimization [23]. Thus, they serve as natural kinematic movement primitives. Interestingly, some curved movements, e.g., in target switching tasks, may be generated from the superposition of straight kinematic motion primitives [21, 28]. Hence, rather than having a concatenation of one stroke after the other, a second movement primitive could be executed while the first one has not yet been completed.

Parabolas, which are equi-affine geodesics [27], are the next set of possible geometric movement primitives. Affine transformations can be used to generate any parabolic stroke from the canonical parabolic template, $y = x^2$, and in order to compactly form a complicated path, a few parabolic strokes can be concatenated. The kinematically defined speed along a parabola reveals an interesting principle. Handzel and Flash [20, 26, 27] have shown that moving at a constant equi-affine speed is equivalent to obeying the two-thirds power law. Following this observation, Polyakov et al. [47, 48] found that the paths of trajectories that obey the two-thirds power law, minimize jerk, and are invariant under equi-affine transformations are parabolic paths.

Interestingly, analysis of monkeys' well-practiced scribbling trajectories has revealed that they are well approximated by long parabolic strokes. Unsupervised segmentation of simultaneously recorded multiple neuron activities using a Hidden Markov model yielded discrete states which when projected on the movement data gave distinct parabolic elements [48, 49]. Moreover, based on the analysis of firing rates of motor cortical neuronal activities recorded from monkeys it was found that the firing of part of the cells is better tuned to equi-affine rather than to Euclidean speed. Thus, the evidence from neurophysiological studies supported the suggestion that parabolas are promising candidates for serving as kinematic motor primitives.

3.3 Mixture of Geometries for Describing Human Behavior

The works of Bennequin et al. [5] and Fuchs [24] included a comparison of the predictions of the mixed geometry model to measured human drawing and walking trajectories, including movements along several predesignated paths. The human paths were segmented according to the kinematic fit given by the trio of mixed geometry parameters. Bennequin et al. [5] compared the human drawings and locomotion trajectories for several shapes against the kinematic predictions of the mixed geometry model. The end-effector trajectories of these movements were segmented by fitting within each segment three constant weights; β_0, β_1, and β_2.

These weights represent the mixture of geometries, i.e. the involvement of the full-affine, equi-affine and Euclidean geometries in the produced kinematics (see Introduction and Bennequin et al. [5]. The weights, that were assumed to be piecewise constant, were derived for various figural forms (cloverleaf, limaçon and lemniscate) and modalities (drawing, locomotion) and then compared according to the distribution of the constant weights (the $\bar{\beta}$ values. Figure 1 depicts the results of fitting a mixture model and the segments that result, based on the notion that within each segment we have constant β values. Figure 1 additionally depicts comparisons between predicted and measured paths and velocity profiles for both drawing (left panel) and locomotion (right panel) trajectories. Figure 2 displays the β values derived for the drawing and locomotion movements. We also present the distribution of the β values derived for the different shapes and tasks (drawing, locomotion). These are presented by the points in the triangles, which are color-coded based on the number of trials optimally fitted by the respective values. A detailed description can be found in Bennequin et al. [5].

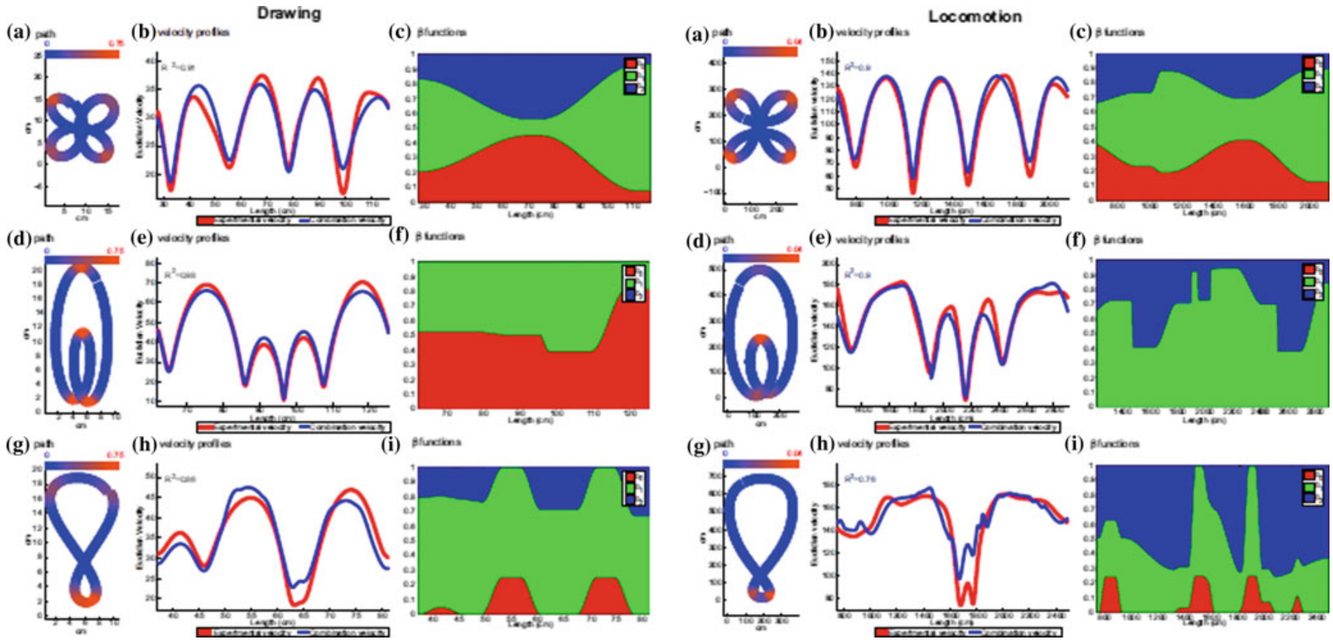

Fig. 1 Mixed geometry modeling of drawing (left panel) and locomotion (right panel) trajectories. Every row shows an example of a path of a drawing (left) and locomotion (right) trials. The shapes include a cloverleaf, an oblate limaçon and an asymmetric lemniscate. Panels (A), (D) and (G) show the paths drawn by the subject. The colors marked on the paths represent the Euclidian curvature. Blue segments have relatively low curvature (0) and red segments have a higher curvature (0.75). Color scale is shown at the top of the panel. Panels (B), (E) and (H) show the velocity profiles of the drawing (left) and locomotion (right). Red, experimental velocity profile; blue, velocity profile predicted by the model of the combination of geometries. Panels (C), (F) and (I) show values of the b functions. Red area, value of the β_0 weight; green area value of the β_1 weight; blue area, value of the β_2 weight. The values are aggregated one above the other such that their sum equals 1

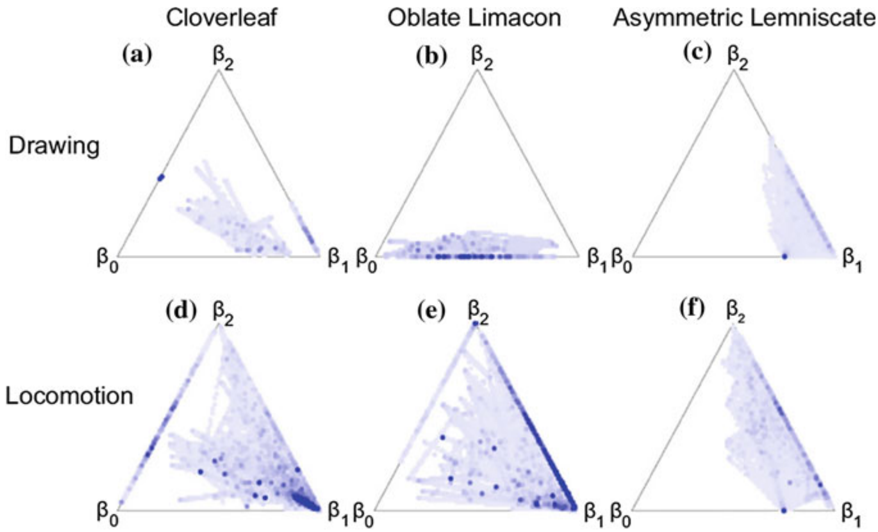

Fig. 2 Representation of the values of the three β weights during the different trials. The distribution of the β weights aggregated over all trials of the same figural form. A point within the triangle gives the values of the β_0, β_1 and β_2 weight parameters where $\beta_0 + \beta_1 + \beta_2 = 1$. The values of β_2 weight function for such a point are equal to the area delineated by the small triangle created by passing lines between this specific point and the two bottom vertices. The values of β_1 are equal to the area delineated by the small triangle created by passing lines between this specific point and the left bottom and top vertices. The values of the β_0 weight function are equal to the area delineated by the small triangle created be passing lines between this point and the right bottom and top vertices. For example, a point on the triangle's edge marked by β_1 is a point where of $\beta_1 = 1$. For a point located at the top vertex, $\beta_2 = 1$ and $\beta_0 = \beta_1 = 0$. In the center of the triangle $\beta_0 = \beta_1 = \beta_2 = \frac{1}{3}$. The color of any point within the large triangle indicates the number of times that that specific combination of β weight values was found. A white point shows a combination that did not appear in any of the trials. A dark blue point represents a combination occurring many times. *Panel (A)* contains all the trials of the drawing of cloverleaves. *Panel (B)* contains all the trials of the drawing of oblate limaçon. *Panel (C)* contains all the trials of the drawing of asymmetric lemniscate. *Panel (D)* contains all the trials of the locomotion of cloverleaves. *Panel (E)* contains all the trials of the locomotion of oblate limaçon. *Panel (F)* contains all the trials of the locomotion of asymmetric lemniscate

3.4 The Geometrical Redundancy in the Mixed Geometry Model

A reexamination of the speed profiles generated by different geometrical mixtures revealed that the mixed geometry model exhibits statistical redundancies [39]; for various paths, it was found that different values of $\bar{\beta}$ trios yield highly similar speed profiles.

For the cloverleaf template, a set of $\bar{\beta}$ trios was found to provide equally good matches ($R^2 > 0.98$) between the mixed geometry model predictions and the experimental data. All these $\bar{\beta}$ trios, which were statistically indistinguishable, obeyed

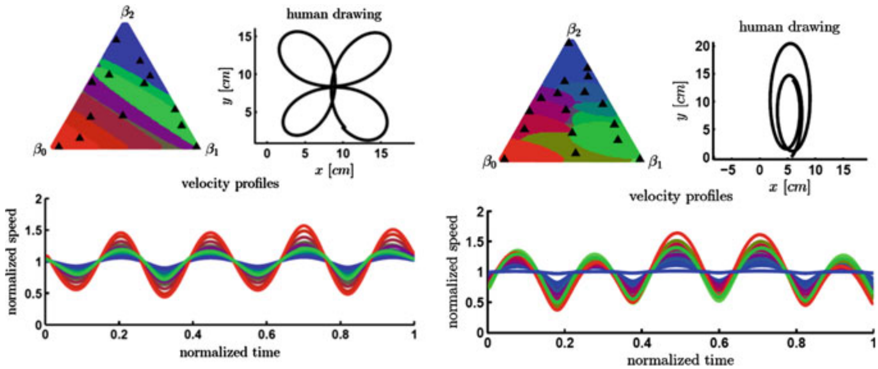

Fig. 3 Redundancy of the mixed geometry model for cloverleafs and limaçons. For each template, the mixed geometry triangle in the *top-left panel* is colored according to the statistical equivalence of parametrizations of the limaçon, the template is drawn on *the top right panel* and *the bottom panel* depicts the different speed profiles that match the different sets of speed profiles. A set of different possible mixtures following a linear relation between β_0 and β_1 yield highly similar results

linear relations between the β_0 and β_1 values, as depicted in Fig. 3. The redundancy map appearing in the upper left panel was calculated by using the following algorithm. The parameter space was quantized by obtaining a discrete set of possible β values that represent distinct, statistically distinguishable speed profiles. The speed profile corresponding to $\beta_1 = 1$ (equi-affine parametrization, or the two-third power law), was calculated and was referred to as the representative profile of the first equivalence group of parameters. Then, all $\bar{\beta}$ weight trios whose speed profiles were statistically indistinguishable from this representative profile were marked as belonging to the first group. A representative for the next equivalence group was chosen as the one giving the best agreement, in terms of R^2, with the previous representative. The process was iterated until all $\bar{\beta}$ weights were examined. Each of the groups for an analytic cloverleaf and the analytic limaçon are shown in Fig. 3, using different patches of color for different equivalent sets.

Thus, the distribution of values appearing in Fig. 2 (taken from [5]) for cloverleaf drawings can be explained by the redundancy map (Fig. 3). We suggest that the control procedure must be invariant with respect to the profiles belonging to the same equivalence class. In particular, the profiles represented in Fig. 3 are all similar from the kinematic output point of view. This suggests that humans may select a straight line in the $\bar{\beta}$ parameters space rather than a unique point. To elucidate whether the redundancy also appears for the real data, the above statistical grouping was also carried out on the actual measured paths. The same statistical tendency as detected for the analytical curves was also seen for the human data, as is shown in Fig. 4.

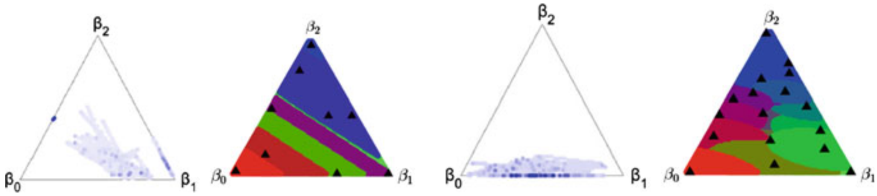

Fig. 4 The variance of the human data presented in the rightmost panel for the cloverleaf is mostly explained by one equivalence set in the second panel from right. Similar results are shown for the limaçon data (the two next panels) which suggests that the different segments in the human data employed mixed geometry weights that are statistically indistinguishable

3.5 Analysis of the Jerk Cost of Mixed Geometry Profiles

While in the above section, we showed that different geometrical mixtures can give rise to required paths; human data show that not all possible $\bar{\beta}$ mixtures within the triangle are used. Notice, however that in the above analysis we did not demand of the resulting velocity profiles to match those observed in human movements. We have shown that when the mixture of geometries model was used to account for the human data, only a subset of possible $\bar{\beta}$ trios was selected. Is it possible that the specific mixtures of geometries being generated are those that optimize behavior?

We inspected which mixtures of geometric speeds yield optimal speed profiles for each predefined movement path [24]. For each geometrical shape, we looked for the unique best geometric mixture describing a full cycle of movement, that yields minimal normalized jerk J_N or normalized acceleration, A_N. We looked for a $\bar{\beta}$ trio that minimizes these costs, but without allowing it to have different segments within a single cycle (one trio accounts for the mixture along the entire path). For this purpose, we calculated J_N for each constant $\bar{\beta}$ trio, for a dense set of $\bar{\beta}$ trios; selecting $\beta_i \in \{0, 0.01, 0.02, , ..0.99, 1\}$. The calculations were made for eight analytically described shapes: one ellipse with eccentricity of 0.97, one cloverleaf, three lemniscates with loop length ratios of 1: 1, 1: 2 and 1: 3 and three limac ons with loop length ratios 1: 3, 1: 5, and 1: 7. We examined the predictions of jerk minimization in explaining the observed parameters of the mixed geometry model. For each movement template we studied what $\bar{\beta}$ trio produces the minimal normalized jerk J_N.

For the ellipse, the J_N minimizing geometrical mixtures had $\beta_2 = 0$ which means that the contribution of the Euclidean geometry had to vanish for this trajectory. Additionally, along an ellipse, the equi-affine curvature is constant. Hence, both full-affine and equi-affine parameterizations result in a $v = \gamma\kappa^{-\frac{1}{3}}$ power law speed profile, and so is the speed profile of their mixture. Hence, analytically the value of the normalized jerk, J_N, is identical for all $\bar{\beta}$ with $\beta_2 = 0$. This case replicates the theoretical predictions of Richardson and Flash [51].

For the lemniscates which have two inflection points and four parabolic points, the set of candidate $\bar{\beta}$ trios for J_N minimization is restricted, because, as was shown above, a parabolic point must have a mixture with $\beta_0 = 0$ and an inflection point must have a mixture with $\beta_1 = 3\beta_0$ [5]. Therefore, we obtain only one feasible $\bar{\beta}$ trio for the entire path (i.e., without segmentation); constant Euclidean velocity, $\beta_2 = 1$.

For the cloverleaf, we found that the optimal geometrical mixture is a linear combination of the geometries, where $\beta_2 = 0.39 - 0.5\beta_1$ in agreement with the prediction of linear combinations from the above statistical analysis of the mixed geometry predictions by Meirovitch [39]. For the limaçon, we found that the optimal geometrical mixture is another linear relation.

These results show that the geometric mixtures yielding the minimal normalized jerk also yield a good description of the geometric mixtures that subjects use for drawing shapes, as long as there are no singularities in the template path. The latter case is likely to require a segmentation of the path into segments according to those singularities.

3.6 Human Data Analysis: Jerk Costs of Movements Arising from Different Geometrical Mixtures

Do the jerk minimizing mixtures match the mixtures selected by the human motor system? For each movement template we looked for the mixture parameter trio $\bar{\beta}$ that minimizes the jerk. The inferred mixtures of geometries derived for different trajectories are shown in Fig. 5 presented in barycentric coordinates. Each panel shows the mixture $\bar{\beta}$ of the different geometries using barycenter positive coordinates $\beta_0, \beta_1, \beta_2$ that produce the minimal normalized jerk J_N for the measured human movement paths. For all movement templates except for the lemniscates, the jerk minimizing parameterization matched human data in drawing them. For the ellipse, the two-thirds power law behavior predicted by jerk minimization is well known to be a good representation of human movement. For the cloverleaf and limaçon the J_N values of subjects' drawings again resembled those obtained from jerk minimization. For the lemniscates, the constant Euclidean speed profile differs significantly from the human speed profiles. This suggests that lemniscates are better represented using some segmentation allowing a change in the $\bar{\beta}$ parameters between consecutive segments. Together, these results show that human movements minimize jerk and that the $\bar{\beta}$ trios, inferred from jerk minimization, are quite similar to those derived from the mixed geometry model, and are showing very similar linear trends between the values of the different β parameters to those observed through the statistical redundancy analysis presented above.

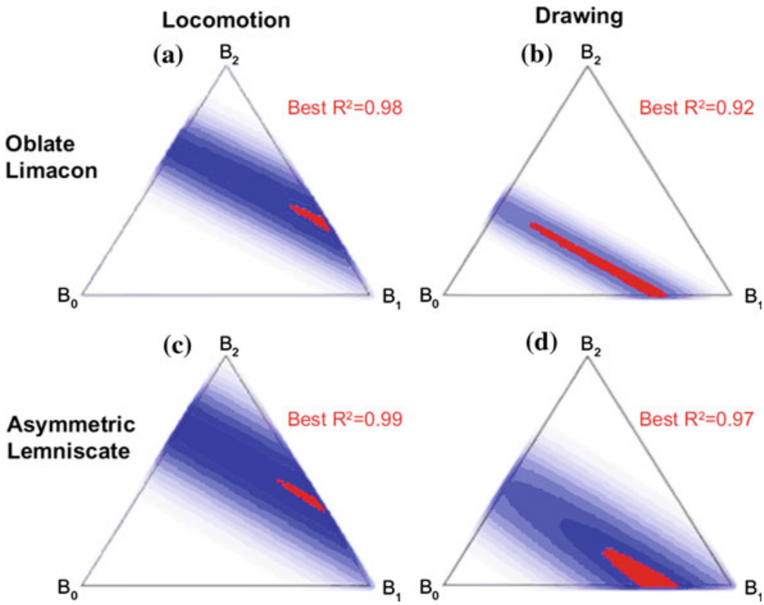

Fig. 5 The triangles show the trios of β parameters obtained from jerk minimization. The color of each point gives the value of the normalized jerk of the velocity profile created by moving along the analytic curve with the geometrical combination that the point represents. The darker a point, the lower the jerk. Red points are those with the lowest jerk

4 Affine Orbits as Geometric Motion Primitives

The suggestion that movements are stereotypical and are constructed through a sequential composition of simple building blocks is a fundamental idea in the study of motor control [22, 23, 35, 43]. The very nature of these building blocks is under debate. Kinematic motion primitives, spatio-temporal building blocks that specify an end-effector movement in time and space, are one possibility of such components. The manner in which the motor system specifies and composes kinematic motion primitives is currently being investigated.

Following Meirovitch [39], we suggest a family of prototypic geometric templates that may serve as motion primitives: affine orbits, which we use in the representation and segmentation of complex human end-effector trajectories. We first describe the properties of affine orbits, then their parameterizations, which provide maximally smooth trajectories, and finally present an algorithm for the segmentation of recorded movement data into geometric affine orbit primitives.

4.1 The Definition and Classification of Affine Orbits

Following Meirovitch [39], we now examine affine orbits, defined as the Lie 1-parameter group orbits of the affine group acting on Euclidean space, Thus each orbit corresponds to a 1-dimensional vector space of the of 2×2 sized matrices, with a single generating matrix

$$A \in gl_2(R),$$

where $A = \begin{bmatrix} a & b \\ c & d \end{bmatrix}$ is a constant matrix, termed the generator matrix.

In general, the Lie algebra of a Lie sub-group of the group of invertible matrices is its tangent space at the Identity matrix; if the sub-group is given by a set of equations, its Lie algebra is defined by taking the common zeros of the differential of these equations. The subspaces V of $gl_2(R)$ that are Lie algebras of some Lie sub-group are characterized by the fact that the bracket $XY - YX$ of any pair of elements X, Y of V also belongs to V. Then, in particular, any sub-vector space of dimension 1 is the Lie algebra of a sub-group, because in this case, X and Y are proportional and the bracket is zero. This subgroup is obtained by exponentiation.

Thus, the resulting trajectory of the affine orbit, $r(\zeta)$ is represented by:

$$r(\zeta) = \exp(A\zeta)p_0,$$

where p_0 is some fixed point in Euclidean space.

The parameter ζ is the orbit's natural arc-length parameter that is specified by the selection of the matrix A. We next examine the relation between this parameter and the geometric canonical parameter and other geometric properties of the curve. The shape of each orbit is dependent on the structure of its generating matrix A. The relation between the structure of A being the group generator and the type of orbit is the following. The Euclidean orbits consist of points, straight lines and circles. A point is the trivial orbit, which is associated with the matrix A being a matrix with 0 values for all its entries (and then its exponent is the identity element of the respective Lie group). Straight lines can be generated by any matrix A with real and identical eigenvalues. Circles are generated by any skew-symmetric matrix A.

Equi-affine orbits generalize the Euclidean ones and include the conic sections: ellipses, hyperboles and parabolas. Ellipses are generated by any matrix A for which $trace(A) = 0$ and $det(A) > 0$. Hyperboles are generated by any matrix A for which $trace\,(A) = 0$ and $det\,(A) < 0$. Parabolas are characterized by an equation defining their eigenvalues; $\alpha = 0$ for α defined as: $\alpha = det(A) - \frac{2}{9}trace^2(A)$. The parameter α is a useful shorthand, and we term it the parabolicity of the affine orbit.

Full-affine orbits are best sorted based on the value of the eigenvalues of A, denoted by λ_1, λ_2. For real eigenvalues, if the matrix is diagonalizable, either both eigenvalues are the same, and the orbit is a straight line or if the eigenvalues are real and different then the orbit can be represented by $y = x^\lambda$, in some x, y coordinate system which is achieved by an affine transformation of the canonical coordinate frame. The latter type of orbit we call here a monomial, although this does not precisely fit this function type. If the eigenvalues are real and the matrix is not diagonalizable, then both eigenvalues are equal, $\lambda_1 = \lambda_2$ and up to a similarity transformation the matrix A is upper triangular with nonzeros above the diagonal). Then the geometric form of the orbit is exceptional; $y = x\log(x)$ for some coordinate frame that results from an affine transformation of the canonical frame. Last, if the two eigenvalues are not real, then they are conjugate and the orbit is an elliptic logarithmic spiral (affine transform of the classical logarithmic spiral).

The different orbits derived in the manner described above are the ones having constant curvatures in their respective geometries; straight lines and circles are the orbits of the Euclidean geometry having constant Euclidean curvatures. Conic sections (parabolas, hyperbolas and ellipses) are the orbits of the equi-affine geometry and have constant equi-affine curvatures, which are 0, negative and positive for these three types of conic sections, respectively (see [20]). All affine orbits have a constant full-affine curvature (for a definition see [5]). The differential properties of an orbit, defined by the geometry, are always continuous functions of the canonical parameter, and on all the orbit's points, the geometric structure is the same up to a transformation by a member of the group.

Olver et al. [44] and Calabi et al. [13] have shown the usefulness of fundamental osculating curves of a given path. They noted that the point-wise geometric properties of the target curve are captured by the respective properties of the osculating one.

Therefore, in each of these geometries: Euclidean, equi-affine and affine, studying the osculating orbits of a general path provides us with the invariants describing the path for the associated geometry.

5 The Geometric Properties of Affine Orbits

5.1 Geometric Curvatures Along Affine Orbits

The affine orbits, being specific paths, enable to represent movement geometry and kinematics in a somewhat simplified form. Their geometric properties, represented by their curvatures, take thus the following form.

The Euclidean, equi-affine, and full-affine curvatures along the orbit at some point p on the orbit are represented by:

$$\kappa = \frac{\left|Ap \times A^2 p\right|}{|Ap|^3}, \quad k_1 = \frac{\alpha}{\left|Ap \times A^2 p\right|^{\frac{2}{3}}}, \quad k_0 = \mp\frac{2}{3}\frac{trace(A)}{|\alpha|^{\frac{1}{2}}},$$

where κ, k_1 and k_0 are the Euclidean, equi-affine and full-affine curvatures, respectively (the parabolicity of the affine orbit, α, was defined in the previous section).

The relation between the full-affine parameter of the orbit ρ and the parameter of the orbit ζ is $\rho = \zeta|\alpha|^{1/2}$.

An exception is the case of a parabola, for which the full-affine curvature is not defined. It can be traversed with equi-affine speed but not with full-affine speed.

5.2 Geometric Speeds Along Affine Orbits

The equi-affine speed along an affine orbit (see definition in Sect. "4.1") is

$$\dot{\sigma} = \exp\left(trace(A)\frac{\zeta}{3}\right)\dot{\zeta}\left|Ap_0 \times A^2 p_0\right|^{1/3}.$$

If $trace(A) = 0$ then the parameter ζ is defining a constant equi-affine speed. Otherwise, the equi-affine speed along an orbit is $d\sigma/dt = 0$. Hence, a constant equi-affine speed along the affine orbit is satisfied by the parameter.

$$\zeta = C_1 \ln|Ap_0 \times A2p_0|^{\left(-\frac{1}{3}\right)}\sigma + C_2.$$

Here C_1 is a geometric constant depending on A and C_2 is an arbitrary integration constant.

The parameterization of an affine orbit (as in Sect. "4.1") with a mixed geometry parameter z, defined for a given mixture trio $\bar{\beta}$ is:

$$dz = C(\bar{\beta})a^{\beta_1}e^{b\beta_1\zeta}|\exp(A\zeta)Ap_0|^{\beta_2}\alpha^{\beta_0/2}d\zeta.$$

Here $C(\bar{\beta})$ is a constant depending on the mixture trio $\bar{\beta}$, and α is the parabolicity constant defined in the previous section, $a = \left|Ap_0 \times A^2 p_0\right|^{1/3}$, and $b = \frac{1}{3}trace(A)$.

5.3 Mixed Geometry Parameterizations of Affine Orbits that Minimize Jerk

We now search for examples for how, using a constant mixture of geometries, one may generate speed profiles and trajectories that are extrema of jerk optimization. We show this for affine orbits.

Bright [12] and Polyakov [47] found analytic expressions for paths along which, when the movement has a constant equi-affine speed, it also yields a minimal jerk cost. Polyakov found that traversing a parabola with constant equi-affine speed yields a minimal jerk trajectory. Bright found a specific spiral for which constant equi-affine speed yields minimal jerk and other spirals for which constant Euclidean or full-affine speed profiles yield minimal jerk trajectories. Because Euclidean, equi-affine and full-affine parameterizations are special cases of the mixed geometry model, our results generalize these previous findings.

5.3.1 Monomials with a Mixed Geometry Parameterization that Minimizes Jerk

We examine monomials, generally defined as affine transformations of the standard Cartesian equation $Y^n = X^m$, for some constant integer exponents n and m. This definition includes as specific examples all parabolic and hyperbolic conic sections. We examine a specific set of monomials, whose generating matrix A is:

$$A = \begin{bmatrix} 1 & b \\ 0 & d \end{bmatrix},$$

where b and d are any real numbers.

We provide a set of mixed geometry parameterizations of monomials that are candidates for yielding jerk extrema. For some finite set of values of the entry d, a mixed geometry solution that minimizes the jerk cost exists. Solutions for the jerk minimizing mixed geometry parameters impose that d satisfies $d = m, n \in \{1, \ldots, 5\}$. These correspond, up to affine transformations, to the free minimum jerk solutions of Flash and Hogan [23]. $Y^n = X^m$, where $n, m \in \{1, \ldots, 5\}$. Each specific solution has a mixed geometry parameterization $\bar{\beta}$ that is a candidate for optimizing jerk along it. As a particular case, this derivation predicts that parabolas should be traversed with equi-affine parameterization in order to minimize jerk. In all of the mixtures derived above, there is no Euclidean contribution (so $\beta_2 = 0$) and the speed profiles are represented by a composition of equi-affine and full-affine parametrizations.

5.3.2 Non-elliptic Logarithmic Spirals, General Mixed Geometry Solutions

If the generator matrix is of the form:

$$A = \begin{bmatrix} 1 & b \\ -b & 1 \end{bmatrix},$$

where b is any real number. Then, any mixture parameter $\bar{\beta}$, (depending on the value of b, the inverse of the orbit rate-of-growth parameter) satisfying:

$$\beta_1 + \frac{2}{3}\beta_2 = \frac{1}{160}(117 + \sqrt{3}C_2 + \left(3858 + 36000b^2 - 120C_1 - \frac{226800}{C_1}b^2 \right.$$
$$\left. - \frac{8760}{C_1} - \frac{96300}{C_1}b^4 + 378000\frac{\sqrt{3}}{C_2}b^2 + 374222\frac{\sqrt{3}}{C_2}\right)^{1/2}),$$

where C_1 and C_2 are constants depending on the parameter b in the above matrix representation of the generating matrix A (defined in [39]) and additionally $1 \geq \beta_i \geq 0$ for all i, is a candidate parametrization for jerk minimization along an affine orbit.

5.3.3 A Mixed Geometry Solution that Is a Candidate on All Non-elliptic Orbits

We now seek a specific mixture parameter that is valid for each non-elliptic orbit that has a generating matrix of the form

$$A = \begin{bmatrix} a & b \\ -b & a \end{bmatrix},$$

where a and b are any real numbers.

The specific trio $\bar{\beta}$, defined by $\beta_0 = \beta_1 = \frac{1}{2}$, is a mixed geometry parameter which guarantees that the first variation of the minimum jerk cost is zero.

5.4 Data Segmentation with Osculating Affine Orbits

We suggest that affine orbits are plausible natural building blocks for the description of trajectories of human movements. We describe here the segmentation algorithm developed by Meirovitch [39] that allows trajectory segmentation using the affine invariant local geometric properties of the trajectory. We examine a set of candidate affine orbits, truncated to form possible movement primitives, whose respective distances from the trajectory are calculated. An optimality criterion is used to select subsets of these primitives that reliably represent the parameterised trajectories [21]. Figure 6 depicts an example of this segmentation for the original and an affine transformed lemniscates.

The following description assumes a sampled trajectory, $r(n) \in R^2, n = 1, \ldots, N$.

For each data point i:

1. We calculate $\psi_i(v)$, the osculating affine orbit.

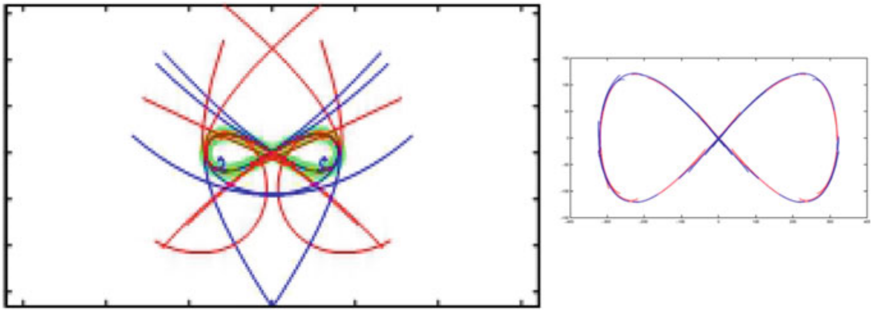

Fig. 6 In the *left panel*, the osculating affine orbits were calculated for every 20th point on one lemniscate, The osculating curves were restricted by a large Hausdorff threshold. Since this metric is not affine invariant the restricted osculating orbit of L1 and L2 differ according to their extent. Each osculation point divided the osculating curve into two branches before and after the point, referred to as "left" (blue) and "right" (red) branches. In the *right panel*, the osculating orbits were calculated and subsequently restricted using a relatively small Hausdorff distance on a scaled lemniscate

2. We then find the maximal boundaries $v_1 < v_2$ such that the one-sided Housdorff distance between the osculating orbit and the curve (taking into account only the distances of points on the orbit from the sampled trajectory) is bounded by a small number ϵ_0

$$Housdorff\left(\{\psi_i(v)\}_{v=v_1}^{v_2}, r(n)_{n=1}^{N}\right) < \epsilon_0.$$

3. We then project the boundaries $\psi_i(v_1)$ and $\psi_i(v_2)$ on the data points $(n1)$, $r(n2)$.
4. Next, we store the value $S_i = (n_1, n_2)$ (overall we will repeat and collect S_i for each of the points on the sampled trajectory $r(n)$).
5. We then use dynamic programming to choose a subset of $\{S_i\}_{i=1}^{N}$ with segments that are compatible with each other (allowing no overlaps of the segments S_i), while maximizing the number of samples in each S_i [37].

The segmentation process is affine invariant, in the sense that the osculating orbits matching an affine transformation of a path are the affine transformations of the osculating orbits matching the original path. This is true except for a minute detail that the trimming of the orbits is based on Euclidean Hausdorff distance which is not affine invariant. Based, however, on numerical simulations, we could conclude that the affine invariance seems to hold, and the segmentation of the affine transformed lemniscate is the affine transformation of the segments of the original lemniscate (Fig. 7).

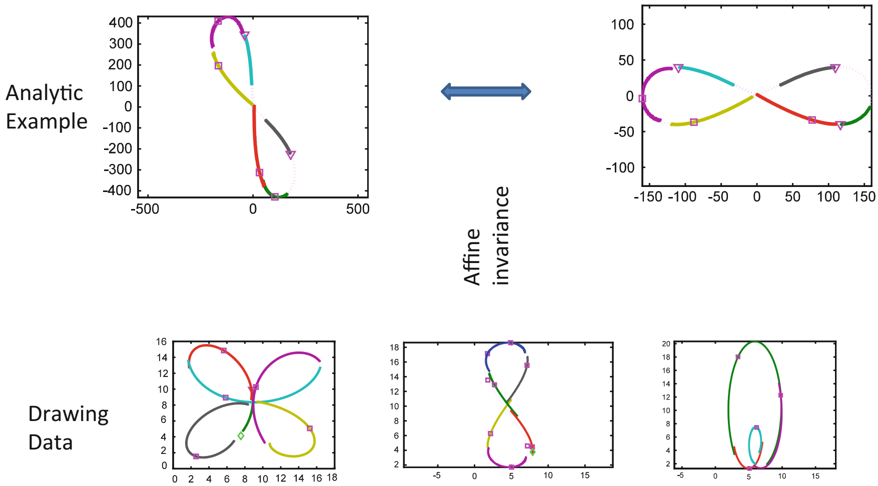

Fig. 7 An optimal segmentation method was adapted and used to select a subset of osculating segments, where for each osculation point three segments were generated according to "left", "right" and "left-right" branches of the osculating curve, where "left-right" included both the "left" and "right" sides of the osculating orbit (see Fig. 6). Triangles, diamonds and squares mark the osculation points in correspondence to whether the selected segments were "left", "right" or "left-right", respectively. The similarity between the segmentations in the two leminscates with respect to the geometry stems from the affine invariance of the osculating orbit. It should be noted that the trimming according to the Hausdorff distance is not an affine invariant, but still under the threshold of the algorithm the difference seems negligible. The colors of the segments are given for the sake of illustration

6 Discussion

In this chapter, we discussed how the concepts of invariance and optimization play different yet complementary roles in the description of how the human motor system plans movement. We examined the mixed geometry model in theory and practice, showing that for some templates a redundancy appears; entirely different mixture parameters produce highly similar speed profiles. Following the results of the mixed geometry model for drawing data, we considered the theoretical aspects of the specific selection of geometric mixtures. First, we noticed that some conditions constrain the space of possible mixtures; singularity points dictate specific mixtures. Next, we reexamined the practical implications of the variety of geometric mixtures. For specific templates, we see that not all mixtures are distinguishable from each other and that different mixtures may yield a similar behavior. We examined the idea that the mixture of geometries may be selected to account for an optimality criterion. Testing various templates reveals that humans select mixtures of geometries that minimize jerk.

We discussed a new theory of motion primitives based on the composition of the classical Euclidean, equi-affine and full-affine geometries [39]. The shapes of these primitives are orbits of 1-parameter subgroups acting on the points in the task space. The non-trivial orbits are straight lines and circles (Euclidean geometry), parabolas, ellipses and hyperbolas (equi-affine geometry), and elliptic logarithmic spirals and monomials (full-affine geometry). After examining the geometric properties and descriptions of the affine orbits, we provide examples of mixed geometry parameterizations of some of these affine orbits that may allow optimal movement along them with respect to jerk minimization.

6.1 Affine Orbits as Motion Primitives

Representing complex movements as a composition of affine orbits that serve as geometrical primitives, is plausible and useful for several reasons.

First, from a theoretical point of view, the geometrical simplicity of orbits makes them attractive candidates for serving as primitives. The symmetry properties of orbits are not only the Euclidean ones obeyed by circles and straight lines, but additionally the non-Euclidean symmetries, that proved to be highly useful in describing the visual properties of shapes in computer vision research [13, 17, 44]. The orbits transform among themselves by specific transformations. Affine mappings permute the set of affine orbits. Any two points along a given orbit can be affinely mapped one upon the other such that the orbit maps to itself. The affine orbits generalize previously suggested movement primitives; straight movement primitives and parabolic movement primitives [23, 48]. Note that a positive direct test of affine invariance reflected in the duration of hand drawings was presented in Pham and Bennequin [45].

Second, we demonstrated some simple mixed geometry parameterizations of affine orbits that may satisfy constrained jerk minimization. This is a generalization of the fact that obeying the two-thirds power law by moving with a constant equi-affine speed along parabolas, automatically minimizes the jerk of the movement [20, 27]. Thus some subsets of geometric primitives are easily assigned with kinematics that are optimal. Additionally, for each affine orbit that is a circular logarithmic spiral, there exists a special mixture of geometries that may minimize the jerk along that orbit.

Third, a movement representation using affine orbits is compact, in the sense that full-affine invariants such as full-affine curvature and arc-length are preserved under affine transformations. The same movement plan, a canonical orbit, can yield different actual paths, according to the affine mapping used in transforming the canonical orbit. Once the shape of primitives is decided upon, the manner of segmenting a movement and extracting these primitives is important. The segmentation algorithm we suggested identifies locally osculating affine orbits and temporally concatenates them as building blocks. The identified set of primitives describing a complex movement is inherently affine invariant. Not only is each primitive by itself affine invariant, but more importantly, a set of concatenated affine orbits describing a path is mapped to a set of affine orbits describing the mapped path. This occurs because osculating affine orbits are mapped to other osculating orbits by affine transformations, unlike best fitting primitives, which are not necessarily mapped to best fitting primitives under affine transformations.

6.2 The Nature of Kinematic Motion Primitives

We now speculate regarding the nature of the motion primitives used by the human motor system.

First, the relation between timing and geometry is unclear. Does the primitive entail a kinematic pattern, or is it just dictating the geometric form? In case that the primitive's description provides only the geometric form, it could be that the timing of motion is dictated at another level, and is possibly selected for the entire composite movement rather than for its primitive components.

Second, the variability of neural patterns and actual movement execution may prove to be an inherent part, dictated by the motion primitives being selected. Perhaps a noisy statistical representation is an essential part of motor execution to the extent that it makes little sense to debate regarding the mean behavior without paying attention to the statistical properties of motor noise. Recently, new statistical frameworks were developed (e.g. [50]) allowing to determine systematic patterns and differences across experimental conditions, participants and repetitions. Such methods are important, since unlike in robotic systems, the physiology of biological systems generates highly variable outputs due to inherent noise in biological sensing of the body and the environment and in the neural commands and muscles' activation patterns underlying motor execution.

Third, a question arises whether human movements are discrete or continuous, i.e. whether they are planned as a whole or by composing together several segments. The notion of a primitive by itself is suggestive of the existence of a set of discrete components that are performed one after the other, or in the case of co-articulation, each starting after the previous one has begun but not necessarily been completed.

Fourth, even if the basic primitives indeed are centrally represented, the manner according to which they are generated may make a large difference. As the human motor system is capable of learning, it is possible that new motion primitives arise when a movement that was previously generated as a concatenation of simpler primitives becomes a single new motion primitive [11, 53]. A process where new primitives emerge out of preexisting ones may also be accompanied by primitive refinement according to some optimality criteria. Thus, a set of previous primitives, first concatenated over time and then adjusted to be molded together and smooth, may form a new motion primitive. This process is interesting when examining movement kinematics but even more so when examining the underlying neural processes.

References

1. Abend, W., Bizzi, E., Morasso, P.: Human arm trajectory formation. Exp. Brain Res. **105**, 331–348 (1982)
2. Abeles, M., Diesmann, M., Flash, T., Geisel, T., Hermann, M., Teicher, M.: Compositionality in neural control: an interdisciplinary study of scribbling movements in primates. Frontiers in computational neuroscience **7**, 103 (2013)
3. Balasubramanian, S., Melendez-Calderon, A., Roby-Brami, A., Burdet, E.: On the analysis of movement smoothness. J. Neuroengineering Rehabil. **12**(1), 112 (2015)
4. Ben-Itzhak, A., Karniel, A.: Minimum acceleration criterion with constraints implies bang-bang control as an underlying principle for optimal trajectories of arm reaching movements. Neural Comput. **20**(3), 779–812 (2008)
5. Bennequin, D., Fuchs, R., Berthoz, A., Flash, T.: Movement timing and invariance arise from several geometries. PLoS Comput. Biol. **5**(7), e1000426 (2009)
6. Bennequin, D., Berthoz, A.: Several geometries for movements generations. In: Laumond, J.-P., Mansard, N., Lasserre, J.-B. (eds.) Geometric and Numerical Foundations of Movements vol. 117, pp. 13–43. Springer Tract in Advanced Robotics (2017)
7. Bernstein, N.: The Co-ordination and Regulation of Movements. Pergamon Press, Oxford (1967)
8. Biess, A., Nagurka, M., Flash, T.: Simulating discrete and rhythmic multi-joint human arm movements by optimisation of nonlinear performance indices. Biol. Cybern. **95**(1), 31–53 (2006)
9. Biess, A., Liebermann, D.G., Flash, T.: A computational model for redundant human three-dimensional pointing movements: integration of independent spatial and temporal motor plans simplifies movement dynamics. J. Neurosci. **27**(48), 13045–13064 (2007)
10. Bizzi, E., Tresch, M.C., Saltiel, P., d Avella, A.: New perspectives on spinal motor systems. Nat. Rev. Neurosci. **1**(2), 101–108 (2000)
11. Bizzi, E., Mussa-Ivaladi, F.A.: Motor learning through the combination of primitives. Philos. Trans. Royal Soc. London Ser. B-Biol. Sci. **355**, 1755–1759 (2000)
12. Bright, I.: Motion planning through optimisation. Master's thesis, Weizmann Institute of Science (2007)
13. Calabi, E., Olver, P.J., Shakiban, C., Tannenbaum, A., Haker, S.: Differential and numerically invariant signature curves applied to object recognition. Int. J. Comput. Vision **26**(2), 107–135 (1998)
14. Desmurget, M., Pélisson, D., Rossetti, Y., Prablanc, C.: From eye to hand: planning goal-directed movements. Neurosci. Biobehav. Rev. **22**(6), 761–788 (1998)
15. de'Sperati, C., Viviani, P.: The relationship between curvature and velocity in two-dimensional smooth pursuit eye movements. J. Neurosci. **17**(10), 3932–3945 (1997)
16. Dingwell, J.B., Mah, C.D., Mussa-Ivaldi, F.A.: Experimentally confirmed mathematical model for human control of a non-rigid object. J. Neurophysiol. **91**(3), 1158–1170 (2004)
17. Faugeras,O., Keriven, R.: (1996) On projective plane curve evolution. In Lecture Notes in Control and Information Sciences, pp. 66–73 (1996)
18. Fitts, P.M.: The information capacity of the human motor system in controlling the amplitude of movement. J. Exp. Psychol. **47**, 381–391 (1954)
19. Flash T.: Organizing principles underlying the formation of hand trajectories. Doctoral dissertation, Massachusetts Institute of Technology, Cambridge, MA (1983)
20. Flash, T., Handzel, A.A.: Affine differential geometry analysis of human arm movements. Biol. Cybern. **96**(6), 577–601 (2007)
21. Flash, T., Henis, E.: Arm trajectory modifications during reaching towards visual targets. J. Cogn. Neurosci. **3**(3), 220–230 (1991)
22. Flash, T., Hochner, B.: Motor primitives in vertebrates and invertebrates. Curr. Opin. Neurobiol. **15**(6), 660–666 (2005)
23. Flash, T., Hogan, N.: The coordination of arm movements—an experimentally confirmed mathematical-model. J. Neurosci. **5**(7), 1688–1703 (1985)

24. Fuchs, R.: Human motor control: geometry, invariants and optimisation, Ph.D. thesis, Department of CS and applied Mathematics, Weizmann Institute of Science, Rehovot, Isreal (2010)
25. Guggenheimer, H.W.: Differential Geometry. Dover Publications, (1977, June)
26. Handzel, A., Flash, T.: Affine differential geometry analysis of human arm trajectories. Abs. Soc. Neurosci. **22** (1996)
27. Handzel, A.A., Flash, T.: Geometric methods in the study of human motor control. Cognitive Studies **6**(3), 309–321 (1999)
28. Henis, E., Flash, T.: Mechanisms underlying the generation of averaged modified trajectories. Biol. Cybern. **72**(5), 407–419 (1995)
29. Hicheur, H., Vieilledent, S., Richardson, M.J.E., Flash, T., Berthoz, A.: Velocity and curvature in human locomotion along complex curved paths: a comparison with hand movements. Exp. Brain Res. **162**(2), 145–154 (2005)
30. Huh, D., Sejnowski, T.J.: Spectrum of power laws for curved hand movements. Proc. Natl. Acad. Sci. **112**(29), E3950–E3958 (2015)
31. Ivanenko, Y.P., Grasso, R., Macellari, V., Lacquaniti, F.: Two-thirds power law in human locomotion: role of ground contact forces. NeuroReport **13**(9), 1171–1174 (2002)
32. Karklinsky, M., Flash, T.: Timing of continuous motor imagery: the two-thirds power law originates in trajectory planning. J. Neurophysiol. **113**(7), 2490–2499 (2015)
33. Kohen, D., Karklinsky, M., Meirovitch, T., Flash T., Shmuelof, L.: The effects of shortening preparation time on the execution of intentionally curved trajectories: optimisation and geometrical analysis. Frontiers Human Neuroscience (in press)
34. Lacquaniti, F., Terzuolo, C., Viviani, P.: The law relating kinematic and figural aspects of drawing movements. Acta Physiol. (Oxf) **54**, 115–130 (1983)
35. Lashley, K.: The problem of serial order in psychology. In: Cerebral mechanisms in behavior. Wiley, New York (1951)
36. Levit-Binnun, N., Schechtman, E., Flash, T.: On the similarities between the perception and production of elliptical trajectories. Exp. Brain Res. **172**(4), 533–555 (2006)
37. Meirovitch, Y: Kinematic Analysis of Israeli Sign Language. Master thesis, The Weizmann Institute (2008)
38. Meirovitch, Y., Bennequin, D., Flash, T.: Geometrical Invariance and Smoothness Maximization for Task-Space Movement Generation. IEEE Trans. Rob. **32**(4), 837–853 (2016)
39. Meirovitch, T.: Movement decomposition and compositionality based on geometric and kinematic principles. Department of Computer Science and Applied Maths Ph. D. dissertation, Weizmann Institute of Science, Rehovot, Israel (2014)
40. Mellinger, D., Kumar, V.: Minimum snap trajectory generation and control for quadrotors. IEEE *Robotics and Automation (ICRA),* pp. 2520–2525, 2011
41. Mombaur, K., Laumond, J.P., Yoshida, E.: An optimal control model unifying holonomic and nonholonomic walking. In: Humanoid Robots. 8th IEEE-RAS International Conference on pp. 646–653 (2008)
42. Morasso, P.: Spatial control of arm movements. Exp. Brain Res. **42**(2), 223–322 (1981)
43. Mussa-Ivaldi, F.A., Solla, S.A.: Neural primitives for motion control. IEEE J. Oceanic Eng. **29**(3), 640–650 (2004)
44. Olver, P.J., Sapiro, G., Tannenbaum, A., et al.: Differential invariant signatures and flows in computer vision: A symmetry group approach. In: Geometry driven diffusion in computer vision (1994)
45. Pham, Q.-C., Bennequin, D.: Affine invariance of human hand movements: a direct test. preprint arXiv Biology:1209.1467 (2012)
46. Pollick, Frank E., Sapiro, Guillermo: Constant affine velocity predicts the 1/3 power law pf planar motion perception and generation. Short Commun. **37**(3), 347–353 (1996)
47. Polyakov, F.: Analysis of monkey scribbles during learning in the framework of models of planar hand motion. Ph.D. thesis, The Weizmann Institute of Science (2001)
48. Polyakov, F., Drori, R., Ben-Shaul, Y., Abeles, M., Flash, T.: A compact representation of drawing movements with sequences of parabolic primitives (2009)

49. Polyakov, F., Stark, E., Drori, R., Abeles, M., Flash, T.: Parabolic movement primitives and cortical states: merging optimality with geometric invariance. Biol. Cybern. **100**(2), 159–184 (2009)
50. Raket, L.L., Grimme, B., Schoner, G., Christian, I., Markussen, B.: Separating timing, movement conditions and individual differences in the analysis of human movement. PLoS Comput. Biol. **12**(9), e1005092 (2016)
51. Richardson, J.M.E., Flash, T.: Comparing smooth arm movements with the two- thirds power law and the related segmented-control hypothesis. J. Neurosci. **22**(18), 8201–8211 (2002)
52. Schaal, S., Sternad, D.: Segmentation of endpoint trajectories does not imply segmented control. Exp. Brain Res. **124**, 118–136 (1999)
53. Sosnik, R., Hauptmann, B., Karni, A., Flash, T.: When practice leads to co-articulation: the evolution of geometrically defined movement primitives. Exp. Brain Res. **156**(4), 422–438 (2004)
54. Tanaka, H., Krakauer, J.W., Qian, N.: An optimization principle for determining movement duration. Neurophysiol. **95**(6), 3875–3886 (2006)
55. Tasko, S.M., Westbury, J.R.: Speed–curvature relations for speech-related articulatory movement. J. Phonetics **32**(1), 65–80 (2004)
56. Todorov, E., Jordan, M.I.: Smoothness maximization along a predefined path accurately predicts the speed profiles of complex arm movements. J. Neurophysiol. **80**, 696–714 (1998)
57. Todorov, E., Jordan, M.I.: Optimal feedback control as a theory of motor coordination. Nat. Neurosci. **5**(11), 1226–1235 (2002)
58. Viviani, P., Cenzato, M.: Segmentation and coupling in complex movements. J. Exp. Psychol. Hum. Percept. Perform. **11**(6), 828–845 (1985)
59. Viviani, P., Stucchi, N.: Biological movements look uniform: evidence of motor-perceptual interactions. J. Exp. Psychol. Hum. Percept. Perform. **18**(3), 603 (1992)
60. Viviani, P., Flash, T.: Minimum-jerk, two-thirds power law, and isochrony: converging approaches to movement planning. J. Exp. Psychol. Hum. Percept. Perform. **21**(1), 32–53 (1995)
61. Vieilledent, S., Kerlirzin, Y., Dalbera, S., Berthoz, A.: Relationship between velocity and curvature of a human locomotor trajectory. Neurosci. Lett. **305**(1), 65–69 (2001)
62. Viviani, P., McCollum, G.: The relation between linear extent and velocity in drawing movements. Neuroscience **10**(1), 211–218 (1983)